Anal. Bioanal. Electrochem., Vol. 16, No. 9, 2024, 830-845
https://www.doi.org/10.22034/abec.2024.716157

Analytical & Bioanalytical Electrochemistry

2024 by CEE
www.abechem.com

Full Paper

Unveiling The Multi Functionality of $CeCuIn_2O_5$ Nanoparticles: A Promising Approach For UV-Light Photocatalysis, Electrochemical Sensing and Antibacterial Applications

M.B. Shivaswamy,[1] H.S. Nagendra Prasad,[1,*] Kiran B. Manjappa,[2,*] S. Madhushree,[1] B.S. Hemanth,[1] B.S. Madhukar,[1] R. Kavya,[1] M.A. Sangamesha,[3] and A.P. Anand[4]

[1]*Department of Chemistry, Sri Jayachamarajendra College of Engineering, JSS Science and Technology University, Mysuru, India-570 006, India*
[2]*Department of Chemistry, Tunghai University, No. 1727, Sec. 4, Taiwan Boulevard, Xitun District, Taichung City 40704, Taiwan, Republic of China*
[3]*Department of Chemistry, The National Institute of Engineering, Mysuru, India-570 00, India*
[4]*Ganesh Consultancy and Analytical Servies, Hebbal Industrial Area, Mysuru, India-570016, India*

*Corresponding Author, Tel.: +91 984 554 0094
E-Mails: nprasad@jssstuniv.in (H.S. Nagendra Prasad); kiran@thu.edu.tw (Kiran B. Manjappa)

Received: 30 March 2024 / Received in revised form: 24 September 2024 / Accepted: 24 September 2024 / Published online: 30 September 2024

Abstract- $CeCuIn_2O_5$ trimetallic oxide nanoparticles (CCI NPs) were synthesised in the current work and examined for antibacterial activity against Methicillin Resistant *Staphylococcus Aureus* (MRSA), photocatalytic degradation of malachite green (MG) and electrochemical sensing of sodium nitrite. The physicochemical characteristics of the CCI NPs were analyzed using XRD, SEM, EDX, UV-vis and DLS method which depicts the morphology, crystalline nature and particle size synthesised CCI NPs. With a linear range of 0.8-4.8mM, the glassy carbon electrode (GCE) modified CCI NPs demonstrated an outstanding electrochemical response for sodium nitrite ($NaNO_2$). In addition, the synthesized CCI NPs showed high photocatalytic activities for the degradation of MG dye in water. It indicates the CCI NPs material produces hydroxyl ($^{\cdot}OH$) and superoxide (O_2^{-}) radicals for MG degradation when exposed to UV light, also showed an efficiency of 89.6% towards the degradation of Malachite Green. Carried out the dose-dependent method to the standard antibiotic streptomycin at 10 g/disc (5, 7, 15, 20, 25 & 30) with a zone of inhibition (ZOI) of 25.27-45.27±0.09 in mm CCI NPs showed excellent antibacterial activity against MRSA in a dose-dependent method. As a consequence, it was found that CCI NPs are an effective multifunctional material that can be scaled up for the quantification of $NaNO_2$, photocatalytic dye degradation of malachite green, and antibacterial activity against MRSA.

Keywords- Trimetallic nanoparticles; Sodium nitrate; Malachite green; Electrochemical sensor; Methicillin-Resistant *Staphylococcus Aureus*

1. INTRODUCTION

Creating various nanomaterials with amazing and unique qualities is undoubtedly a trailblazing approach to addressing the problems in renewable energy, human health, advanced medical techniques, and challenges in medical treatments. However, not many reports to address these specific problems are available. Because of their extraordinary chemical, biological, and physical characteristics, nanoparticles (NPs) [1-3] have been applied in widespread technologies, in a range of sectors [4,5]. The number of metal mixes determines the classification of metal oxide nanoparticles (NPs) into mono, bi, and trimetallic classes [6] they consist in which transition metallic NPs exhibit greater catalytic activity in a variety of organic transformations [7,8]. Recently, employing trimetallic NPs has considerably gained attention due to their novel physical and chemical characteristics produced by the complementary properties of the monometallic equivalents, particularly in catalytic systems [9]. As a result, compared to mono and bimetallic, trimetallic NPs have frequently shown broad application potential in a range of fields [10,11].

Environmental, nutritional, industrial, and physiological systems all include significant amounts of nitrate ions as a result of human activity and the natural nitrogen cycle. Excessive nitrate levels in water have been linked to physiological and environmental issues, according to several research [12,13]. The World Health Organisation (WHO) advises against exceeding 11 mg/l of nitrate in drinking water because of possible health risks. Thus, it is essential to keep an eye on the nitrate levels in water [14]. To detect and remove the toxins from the wastewater, metal-based sensing, composite materials adsorption, and photocatalysis are being widely used. Photocatalysis is considered to be the most practical approach to removing organic pollutants from contaminated water. However, to detect and quantification of nitrate levels in water, Numerous techniques have been developed. Recently, because of their excellent sensitivity and precision, sensors have been used to measure nitrate at a low level. Potential nitrate-detecting materials have included doped polypyrrole nanowires, nitrate reductase enzymes, copper, silver, platinum, palladium, and platinum-palladium alloys [15,16]. Conversely, nanoparticles (NPs) have become an essential component of contemporary medicine, since they are among the options that may be brought about by the production of reactive oxygen species (ROS) on the produced nanomaterial [17,18]. Among others, effective antibacterial and anticancer drugs are made from silver, palladium, gold, indium, nickel, copper, and cerium nanoparticles [19,20]. Herein we would like to report the synthesis and multifunctional ability of $CeCuIn_2O_5$ trimetallic oxide nanoparticles (CCI NPs). The prepared NPs were successfully employed in photocatalysis to degrade the MG dye in water, electro

sense towards the nitrate, and antibacterial properties against Methicillin-Resistant *Staphylococcus Aureus.*

2. EXPERIMENTAL SECTION

All the materials used for the manufacturing of CCI NPs are analytical grade and purchased from Sigma Aldrich. Throughout the experiment, deionized (DI) water is consumed. Using a Shimadzu UV1800 spectrometer, the absorbance of the synthesised nanoparticles was determined. A Cu Kα radiation-equipped X-ray diffractometer (proto-A-XRD, Canada) was used to determine the crystal structure, with a λ value of 1.5406 Å. Trimetallic oxide nanoparticles were analysed using Zeiss EVO LS15 equipment, which acquired images from a scanning electron microscope (SEM), an energy dispersion X-ray analyser (EDAX), and elemental mapping. The dynamic light scattering (DLS) was measured using the nanoparticles at 25°C using a Malvern Zeta sizer Nano ZS-90 (Malvern Instrument, UK) apparatus. The CH electrochemical analyser (CHI 750 D) was used for the electrochemical sensor experiment. With a scan rate of 0.1 mVs^{-1}, potassium chloride (pH 7) was employed as a supporting electrolyte.

2.1. Synthesis of CCI nanoparticle

Indium(III)nitrate ($In(NO_3)_3$), cerium(III)nitrate ($Ce(NO_3)_3$), copper(I)nitrate ($CuNO_3$), and glycine were used for the formation of trimetallic nanoparticles. Using a magnetic stirrer, a calculated amount of 1.2 g of $In(NO_3)_3$ (0.4 M), 1.3 g of $Ce(NO_3)_3$ (0.3 M), and 0.37 g of $CuNO_3$ (0.5 M) were dissolved in 30 mL of DI water. The mixture was then swirled for 60 minutes at 50 °C. The solution quickly changed colour from light black to dark after the cautious addition of 10 mL of glycine. Throughout the procedure, the solution's basic pH was maintained by sporadically adding ammonia solution (~1 mL). Following the mixture's viscous development, it was carefully transferred to a heated silica crucible and calcined for four hours at 800°C. The resulting metal oxide was subsequently crushed into a fine powder and stored in a desiccator for further uses [21].

2.2. Preparation of electrodes for electrochemical studies and sensors

Trimetallic oxide nanoparticles (CCI NPs) assisted detection of nitrate (NO_2) and electrochemical sensor activities were performed using computer-controlled CHI 750 D Electrochemical sensor workstation three electrode systems— Ag/AgCl serves as the reference electrode, platinum wire serves as the counter electrode, and the modified Glassy Carbon Electrode (GCE) serves as the working electrode were used in the examination. Before the experiments, the working electrode was cleaned with alumina slurries (0.3, 0.1, and 0.05 µm), washed with DI water, and then prepared CCI NPs (1 mg in 5 ml of water) were drop-cast onto

the surface of the polished working electrode and dried in the sun. Further, the modified CCI NPs/GCE working electrode was immersed in KCl (0.05M) and buffer (pH 7) solution (6 mL) during the electrochemical sensor studies [22].

2.3. Photocatalytic degradation of malachite green

A specific amount of CCI NPs is added to a 100 mL malachite green (MG) aqueous solution, and the entire mixture was agitated for up to 120 minutes while being exposed to 18 watts of UV light. In the meantime, sporadic additions of NaOH (0.01 N) and HCl (0.01 N) solution helped to maintain the pH of the mixture. The photodegradation's development was tracked at different intervals. Centrifugation (2500 RPM, 10 min), filtration, and UV-vis spectroscopy analysis are the usual procedures used in sample analysis. At λ_{max} = 540 nm, the amount of MG in every sample of deteriorated water was assessed. A standard curve was given, which plotted absorbance against various MG concentrations at λ_{max}. To calculate the photocatalytic degradation efficiency, employ Equation (1).

$$x = \frac{C_0 - C_t}{C_t} x100\% \qquad \text{Eq. (1)}$$

Where, C_0 and C_t represent the concertation of malachite green at initial and at certain interval respectively [23]. The detailed summary of the photodegradation of the MG dye is presented in Table 1.

Table 1. The conditions of the photodegradation

Parameter	Value
CCI NPs dosage	10-40 mg
Dye concentration	5-20 PPM
pH	4-9
Temperature	Room temperature (22-26ºC)
Irradiation duration	Up to 120 min

3. RESULTS AND DISCUSSION

3.1. Characterization

3.1.1. X-ray diffraction analysis (XRD)

The XRD profile of the prepared CCI NPs are shown in Figure 1. The In*(222), In*(400), In*(440), and In*(622) planes correspond to the peaks that emerge at 2θ = 30.40º, 35.56º, 51.18º, and 60.77º, respectively (JCPDS No. 04-2195). The planes Ce#(111), Ce#(200), Ce#(220), and Ce#(311), respectively, are in good agreement with the peaks that emerge at 2θ = 28.76º, 33.41º, 47.61º, and 56.51º (JCPDS No. 04-0394). According to JCPDS No. 04-0836, the CuΔ(200), CuΔ(112), CuΔ(020), and CuΔ(113) planes emerged at 2θ = 38.84º, 45.81º, 51.18º, and 69.69º, respectively [24-26].

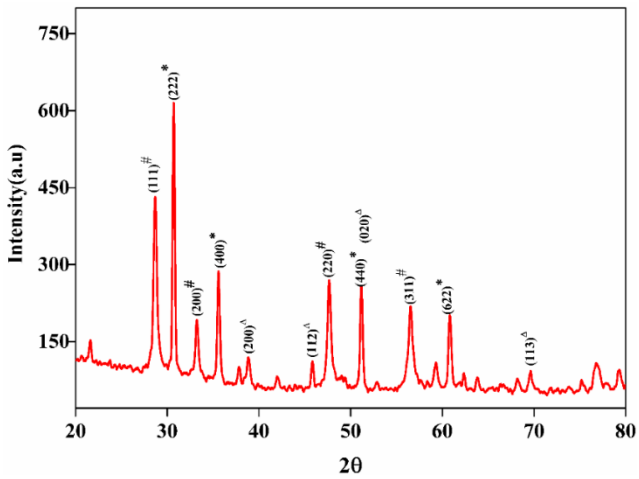

Figure 1. XRD pattern of the synthesised CCI NPs

The crystal domain size (D) of the CCI NPs is computed using Scherrer's relation to rationalise the microcrystalline parameter. The Scherrer's length, which is listed in Table 2, varies from 58 to 65 nm and it was good agreement with the DLS result.

$$D = \frac{0.94\lambda}{\beta * \mathrm{Cos}\,\theta} \qquad \text{Eq. (2)}$$

where λ is the wavelength of the X-rays used, θ is the diffraction angle, and β is the full width half maximum (FWHM). D is the average crystal domain size perpendicular to reflecting planes.

Table 2. Scherrer's length data of the synthesised CCI NPs

Serial number	2θ	β (FWHM)	Scherrer length (nm)
I.	30.67	0.237	63.33
II.	35.51	0.249	61.04
III.	51.12	0.2702	59.38
IV.	60.17	0.2796	59.83

3.1.2. UV-visible spectroscopy analysis (UV-vis)

The UV-vis spectra were acquired in a solution phase by dissolving 0.5 mg of CCI NPs in 5 ml of isopropyl alcohol. The absorption profile shows a broad shoulder ranging from 280-580 nm where absorption around 363, 310, and 338 nm corresponds to the presence of CeO_2, CuO, and In_2O_3 nanoparticles [27-29]. From the tauc plot of $(\alpha h\upsilon)^2$ vs. $h\upsilon$ for nanomaterial, optical bandgap (Eg) for CCI NPs was calculated using Eq. (3), and the value was found to be 3.3eV [30].

$$(\alpha h\upsilon)^2 = a(h\upsilon - Eg) \qquad \text{Eq. (3)}$$

Where υ is the frequency, h is the incoming photon's energy, α is the absorption coefficient, and h is the Planck constant. Furthermore, the synthesised nanoparticles aptitude for dye degradation is confirmed by the observed energy gap derived from the absorption spectrum data. Figure 2 records and displays the synthesised CCI NPs' UV-vis absorption profile.

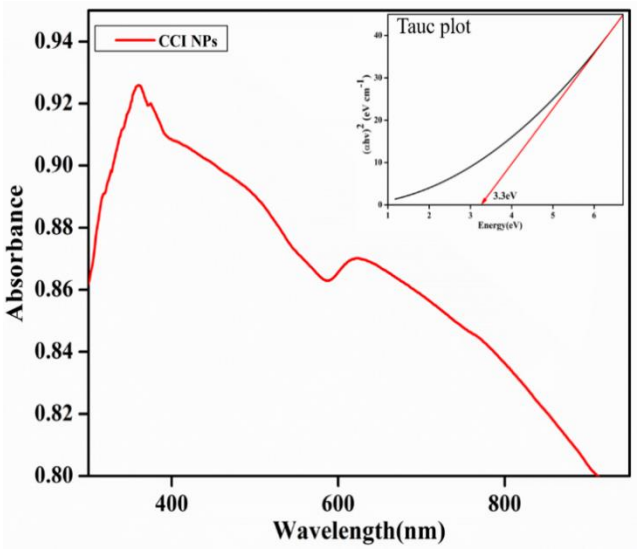

Figure 2. UV–vis spectra of the synthesised 0.5 mg CCI NPs in a 5ml of isopropyl alcohol

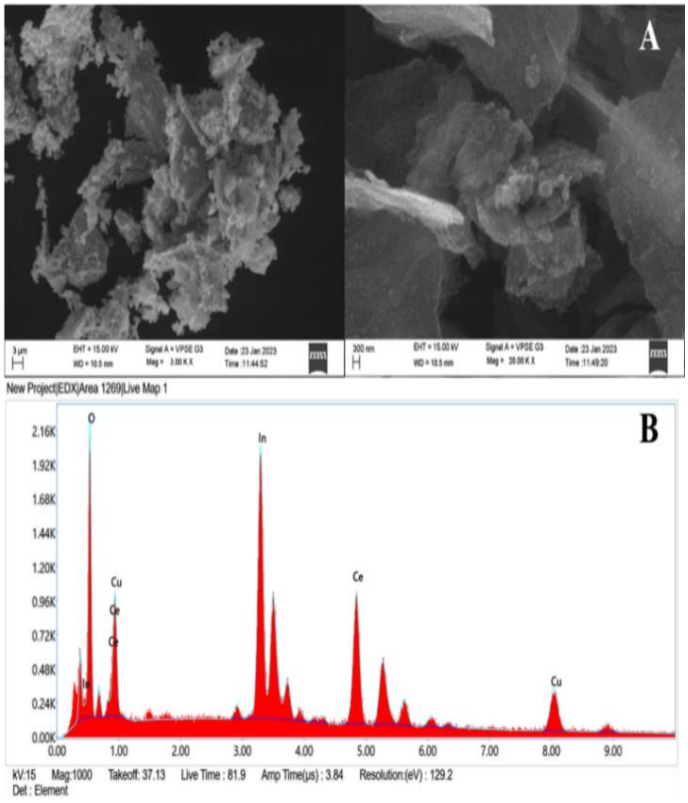

Figure 3. A) Scanning Electron Microscope and B) EDAX spectrum of synthesized CCI NPs

3.1.3. Scanning electron microscopy and Energy dispersive X-ray analysis (SEM-EDX)

To investigate the surface topography and grain size of the synthesized CCI NPs, SEM was employed. The SEM microphotograph clearly showed that the synthesized CCI NPs are irregular in form. The elemental composition of produced CCI Nanoparticles was further validated by EDX and found to be 30.4, 35.6, and 17.8 wt% for indium, cerium, and copper respectively. This examination demonstrates that no other elemental peaks associated with impurities are present in the prepared CCI NPs [31]. Figure 3 and 4 depicts the SEM images and EDAX profile of the prepared CCI NPs.

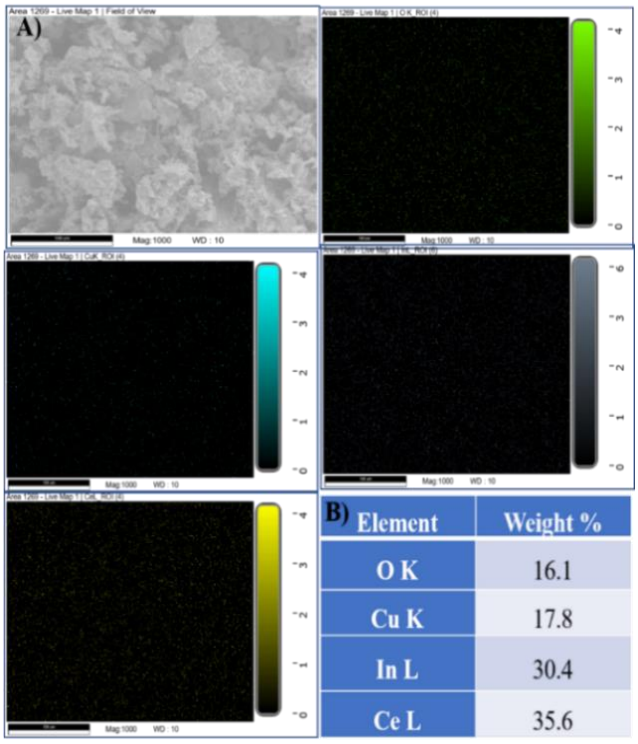

Figure 4. A) EDAX elemental mapping of CCI NPs; B) Elemental composition obtained from EDAX of CCI NPs

3.1.4. Dynamic Light Scattering analysis (DLS)

CCI NPs size was determined using a particle size analyser and the dynamic light scattering technique. The nanoparticles zeta potential has been shown to be -0.1 mV, and their average particle size determined is 64.9 nm. Thankfully, these numbers match the Scherer's length computation figures obtained from the XRD investigation [32]. The particle size graph for CCI NP that was produced using the DLS approach is shown in Figure 5.

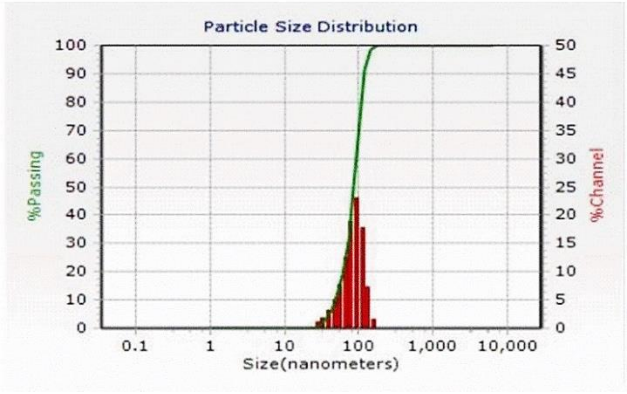

Figure 5. Particle size distribution graph of CCI NPs by DLS

3.2. Electrochemical sensor analysis

Cyclovoltammetry (CV) experiments were used to ascertain the charge efficiency and reversibility of the modified electrodes response. $NaNO_2$ (0.8 mM) was employed as the analyte, and the glass carbon electrode (GCE) was utilized as the working electrode. The potential was adjusted between -1.2 V and +1.2 V, and the scan speeds ranged from 0.05 mV/s to 0.25mV/s. Cyclic voltammogram of the conducted studies are presented in Figure 6A and 6B. From the CV studies it is obvious that bare GCE showed current response in the potential window between -0.1 V and 0.2 V, which is probably due to electrooxidation of the nanoparticles [33,34].

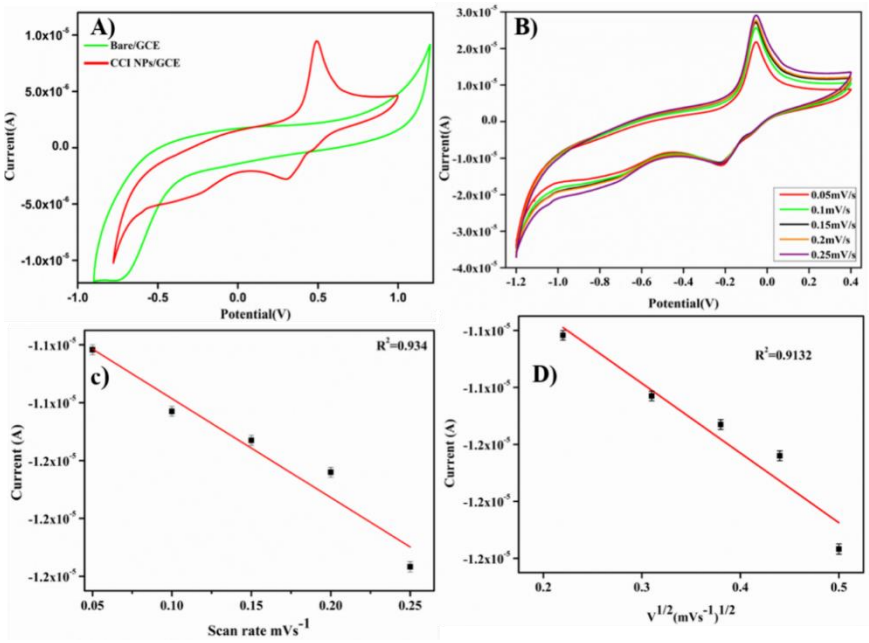

Figure 6. A) CV graph of GCE and CCI/GCE in 0.8mM $NaNO_2$; B) CV graph of CCI NPs/GCE at different scan rates (0.05 mV/s to 0.25 mV/s) calibration plot of C) peak current *vs*. scan rate and D) peak current *vs*. square root of scan rate

However, CCI NP coated GCE showed current response between 0.05mV and 0.25mV, depending on the scan rate. The fast electron transfer of kinetics CCI nanoparticles in the presence of analyte resulted in an apparent increase in current sensitivity [35,36]. Figure 6C's plot of scan rate vs peak current shows a strong linear connection between both of them, with a coefficient of regression of 0.934. Furthermore, using a comparable CV data set, a correlation between the peak current and the square root of the potential scan rate was found. Figure 6D displays an excellent linear connection between peak current and square root of scan rate, with a regression value of 0.9132. presently a graph of peak current (I_p) *vs*. log scan rate (v) is studied and the slope value is almost equal to 1, then it obeys the diffusion-controlled processes [37].

Applications for electrochemically aided sensing are thought to be more precise and dependable. Hence, a linear sweep voltammetry approach has been employed to examine the generated CCI NPs suitability for sensing applications. The studies were carried out at pH 7 using sodium nitrate (0.8–4.8 mM). Figure 7A&B illustrates the relationship between the measured peak current values and the nitrate content. The lowest concentration (0.8 mM) showed an electrochemical response throughout the investigation, which would have suggested the presence of complex nanostructured CCI NP encapsulated on to GCE. Over the entire range of concentrations, the resulting dependence is linear [38]. The electrochemical behaviour of $NaNO_2$ is known to be significantly influenced by pH. The effects of pH on $NaNO_2$ peak current were investigated using CVs in 0.05 M KCl with 0.8 mM $NaNO_2$ and a pH range of 3 to 11. Figure 7C peak current against pH graph shows how the redox peak current gradually increases as pH values climb from 3 to 7.

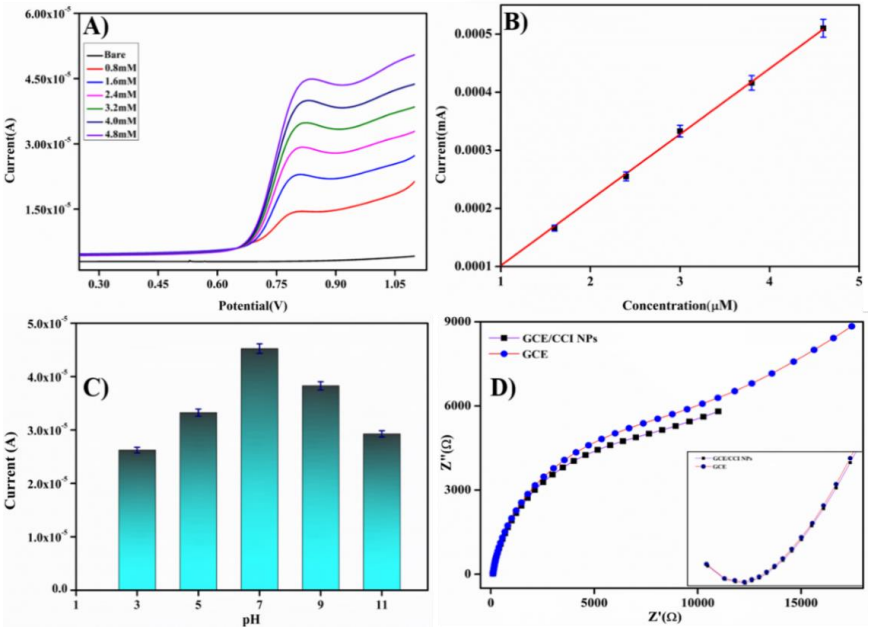

Figure 7. A) LSV graph of the sodium nitrate at different scan rate (0.8-4.6 mM) in CCI NPs/GCE electrode; B) Calibration plot of concentration of sodium nitrate; C) pH impact on CCI NPs modified GCE and GCE; D) EIS spectra of GCE and GCE/CCI NPs

Additionally, as pH levels climb above 7, the peak current falls. The largest peak current of $NaNO_2$ was observed in pH 7, suggesting that electrochemical redox process of sodium nitrate is pH-sensitive. Consequently, 0.05 M KCl at pH 7 served as the supporting electrolyte for the subsequent electrochemical sensor tests. As shown in Figure 7D, Electrochemical impedance spectroscopy is the valuable method for examining the surface-modified electrodes across surfaces properties. Important information on impedance change at the electrode surface is provided by EIS. The frequency range of an open-circuit design using the EIS approach is 1 Hz to 100,000 Hz. Both the GCE and the CCI NPs modified GCE display the charge transfer resistance as a semicircle diameter; however, in contrast to the GCE, the CCI NPs modified electrode displays the solution resistance as an intersecting curve on the actual section at a high frequency [39].

Redox peak currents were recorded under comparable circumstances on the first to fifteenth days of storage in order to assess the stability of the CCI NPs. As shown in Figure 8A, where the plot of percentage current vs. number of days shows a retained current response of 100%, 98.5%, 97.4%, 95.5%, 93.8%, 91.15%, 88.5%, and 85.05% in contrast to the initial current response, the CCI NPs appear to remain stable for at least 12 to 15 days. for repeatability test five sets of CCI NPs/GCE that have been developed. Figure 8B displays the current response for each of the five CCI NPs/GCE electrodes. The low magnitude variation clearly demonstrates the CCI NPs exceptionally good repeatability.

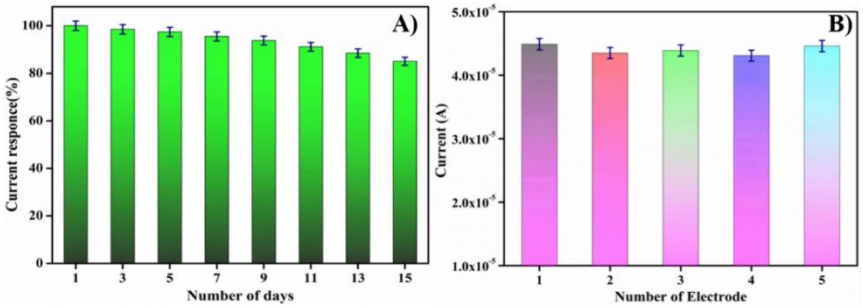

Figure 8. A) Stability of CCI NPs for the detection of $NaNO_2$; B) The repeatability studies at CCI NPs

3.3. Photocatalytic degradation

Synthesised CCI NPs were used to study the degradation of malachite green (MG) dyes. Figure 9. shows that peak of MG absorption in aqueous was measured at 613nm. Following the addition of CCI nanoparticles as a catalyst, the MG colour changed every ten minutes and the absorbance spectra of MG gradually dropped. As can be shown in Figure 9, 40 mg of CCI NPs is enough to eliminate 89.6% of MG dye in intervals of 80 minutes (Supplementary Table 1). Results indicate that the produced CCI NPs are a more potent and efficient catalyst for minimising the concentration of dangerous MG dyes [40].

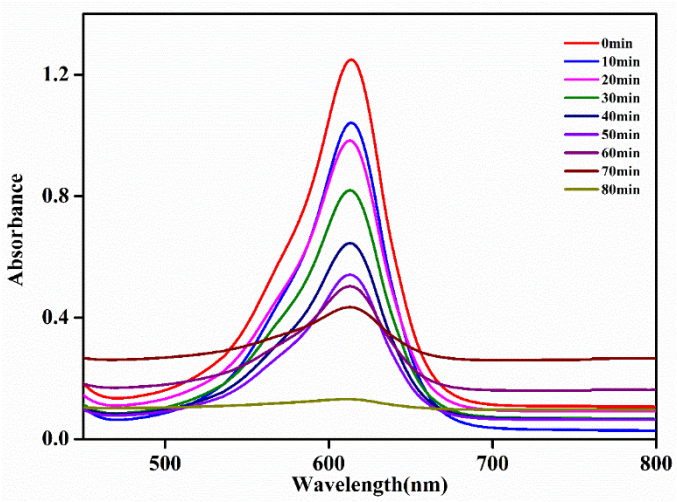

Figure 9. Malachite green absorption dye degradation at 10-minute intervals (5 mg MG dye in 40 mg CCI NPs at pH 7)

Figure 10A displays how the catalytic load affects the MG dye degradation. The optimal catalyst dosage was found by increasing the catalytic load from 10 mg to 50 mg. The concentration of the catalyst causes its active sites to rise; at 40 mg, they max. The aforementioned analytical result indicated that the optimal load was 40 mg of dye at 5 ppm [41]. Figure 10B shows how different dye concentrations affect the photocatalytic activity of CCI NPs. The experimental dye concentration was varied from 5 to 20 ppm, while the NPs amount was maintained at constant (40 mg). According to the testing results, the optimal load was 40 mg for 5 ppm dye because it was completely degrading within a 90-minute interval of time.

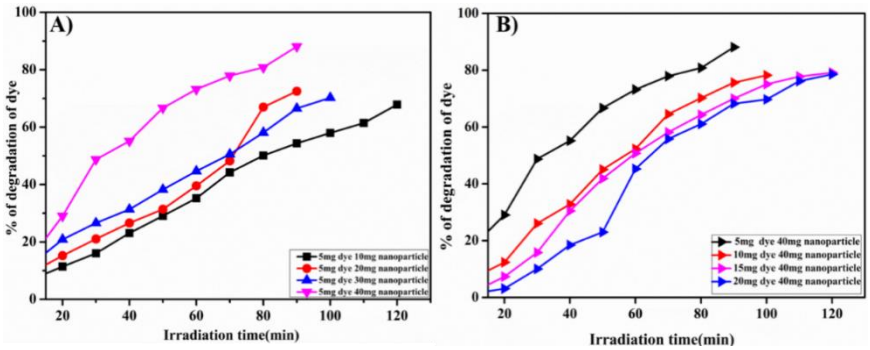

Figure 10. A) Impact of varying nanoparticle concentrations on catalytic degradation; B) Different dye concentrations effects on control nanoparticles

Figure 11 shows how pH affects 40 mg of nanoparticles photo catalytically degrading 5 ppm of MG dye. The graphic clearly shows how important is effect of pH on dye solution in the photocatalytic process. To change the pH, add 0.05 M H_2SO_4 or 0.05 M NaOH to the mixture. Figure 11A makes it clear that MG dye degrades rapidly more quickly in basic

solution at pH -9 than it does at pH 4,5, and 6. Furthermore, in 40 minutes, MG dye will break down in the basic medium at a rate of 89.6%. pH modifies the trimetallic surface properties, facilitating easier dye molecule separation [42]. CCI NPs had an 89.6 degradation percentage, a regression coefficient (R^2) of 0.993, and a rate constant of 0.00712 min^{-1}, as shown in Figure 11B.

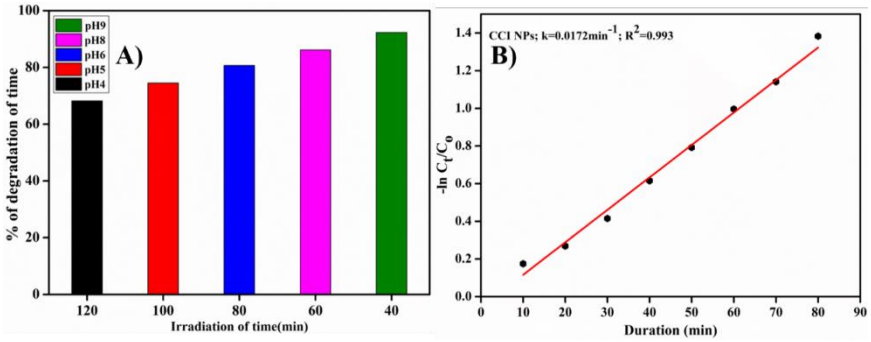

Figure 11. A) pH effect on the MG dye degradation and B) Pseudo first order kinetics and rate constants of the MG dye degradation

It was also observed that the pseudo-first-order kinetics equation matched the promising regression coefficient values. As a result, CCI NPs work in concert to promote increased light absorption and quicker charge separation, which accelerates the MG dye degradation [43].

3.3.1. Mechanism of Photocatalytic degradation

Figure 12. depicts the overall process of photocatalytic activity. Positive holes are left behind when electrons in a material respond to UV photons with energy equal to or greater than the band gap of that material by moving from the conduction band (CB) to the valence band (VB). We call this process the reduction stage. $O_2^{\bullet-}$ and $OH^{\bullet}$ (oxidation) are examples of reactive oxygen species (ROS), which are created when reduction produces electrons and holes. One important side effect of photocatalysis is the generation of ROS, which can cause dye degradation.

It is evident from the UV data that the synthesized nanoparticles show the band gap energy of CCI NPs is 3.3eV, which is equivalent for the wavelength of UV radiation.

These equations (4,5,6 and 7) provide a summary of the most likely responses [44].

$$CCI\ NPs + h\nu \rightarrow CCI\ NPs + h^+ + e^- \quad \text{Eq (4)}$$

$$h^+ + H_2O \rightarrow OH + H^+ \quad \text{Eq (5)}$$

$$e^- + O_2 \rightarrow O^{-2} \rightarrow OH^- \quad \text{Eq (6)}$$

$$OH/\ O^{-2}/\ h^+ + AC \rightarrow \text{Degradation intermediates} + CO_2 + H_2O + \text{etc.} \quad \text{Eq (7)}$$

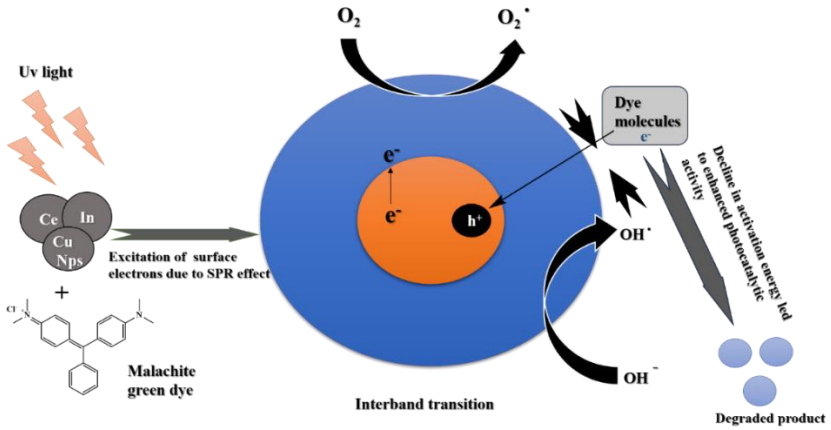

Figure 12. Diagrammatic illustration of the probable photocatalytic dye degradation mechanism

3.4. Antibacterial studies

Methicillin-resistant *Staphylococcus aureus* (MRSA) was used to test the antibacterial activity of CCI NPs. In a dose-dependent manner (5,7,15,20,25, & 30 µg/mL), CCI NPs demonstrated excellent antimicrobial properties against MRSA with ZOI of 25.27±0.06, 29.31±0.12, 30.45±0.14, 34.56±0.12, 39.41±0.16, 40.14±0.21, and 45.27±0.09, in comparison to the standard antibiotic streptomycin (17.70 ±0.05mm Zone of inhibition) (Supplementary Figure S1).

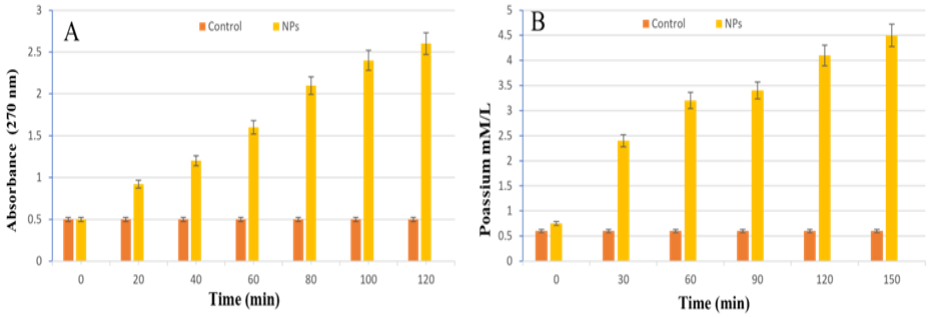

Figure 13. A) MRSA cell membrane damage test validity is verified by DNA leakage from cells and B) Measurement of potassium level in suspension detected after CCI NP treatment

3.4.1. Cell damage by cellular leakage of MRSA membrane and potassium efflux

MRSA cells treated with CCI NPs at their minimum inhibitory concentration (MIC) were used in the experiment; untreated culture served as the control. Cell membrane damage is demonstrated by changes in potassium efflux, as seen in Figures 13A and 13B. By raising the dosage of CCI NPs in tandem with a rise in cellular leakage and potassium content in the solution, cell damage may also be confirmed.

4. CONCLUSION

The development of a long-term substitute material for handling analytical measures, organic pollutants and health care is one of the most important research demands. The current work demonstrates how to create ecologically friendly and cost-effective trimetallic oxide nanoparticles for application in healthcare and the environment by combining ($Ce(NO_3)_3$), ($CuNO_3$), and ($In(NO_3)_3$). The sensitive electrochemical probe CCI NPs is useful for detecting $NaNO_2$ in water samples. It has also been found to promote the breakdown of malachite green (MG) via UV-active photocatalysis and to have antibacterial properties against MRSA. For analysing the electrochemical sensor's $NaNO_2$ recovery from actual samples, the selectivity, repeatability, and shelf life were thoroughly evaluated. Additionally, 40 mg of synthesised CCI NPs were tested to determine the ideal concentration for photocatalytic MG degradation at 5 ppm; the results showed an 89.6% degradation rate at pH 9 in 40 minutes. Moreover, CCI NPs demonstrated a dose-dependent superiority over the conventional antibiotic streptomycin (17.70±0.05 mm Zone of Inhibition (ZOI)) at 10 µg/disc. Consequently, the dual importance of CCI NPs for medicinal and environmental applications is made clear by their use in industry.

Acknowledgments

The authors express their sincere gratitude to Sri Jayachamarajendra College of Engineering (SJCE), JSS Science and Technology University, Mysuru and Ganesh Consultancy & Analytical Services, Mysuru, for providing instrumentation facilities.

Declarations of interest

The authors declare no conflict of interest in this reported work.

Supplementary file information

The materials, methodology, results, and discussions for the antibacterial studies are added to the supplementary file and given the title "Supplementary File."

REFERENCES

[1] M.A. Mahmoud, B.R. Alsehli, M.T. Alotaibi, M. Hosni, and A. Shahat, Environ. Sci. Pollut. Res. Int. 31 (2024) 3466.
[2] M.N. Nadagouda, and R. S. Varma, Green Chem. 8 (2006) 516.
[3] R.P. Rao, S. Mishra, R.M. Tripathi, and S.K. Jain, Inorganic Nanometal Chem. (2021) 1.
[4] S. Iravani, and R.S. Varma, ACS Sustain. ACS Sustainable Chem & Eng. 8 (2020) 5395.
[5] M. Nasrollahzadeh, M. Sajjadi, S. Iravani, and R.S. Varma, Nanomaterials 10 (2020) 1784.

[6] P. Venkatesan, and J. Santhanalakshmi, Langmuir 26 (2010) 12225.
[7] N. Basavegowda, K. Mishra, and Y.R. Lee, J. Alloys Compd. 701 (2017) 456.
[8] B.N. Mondal, A. Basumallick, and P.P. Chattopadhyay, J. Alloys Compd. 457 (2008) 10
[9] J.H. Park, and H.S. Ahn, Appl. Surf. Sci. 504 (2020) 144517.
[10] G. Sharma, S. Bhogal, V.K. Gupta, S. Agarwal, A. Kumar, and D. Pathania, J. Mol. Liquids 275 (2019) 499.
[11] M. Kgatle, K. Sikhwivhilu, G. Ndlovu, and N. Moloto, Catalysts 11 (2021) 428.
[12] R. Desai, M. Marti Villalba, N.S. Lawrence, and J. Davis, Electroynalysis 21 (2009) 789.
[13] Guidelines for drinking water quality recommendations (World Health Organization Press, Geneva, 2004, 3rd edn).
[14] J. Davis, M.J. Moorcroft, S.J. Wilkins, R.G. Compton, and M.F. Cardosi, Analyst 125 (2020) 737.
[15] S. Aravamudhan, and S. Bhansali, Sensors and Actuators B: Chem. 132 (2018) 623.
[16] Y. Li, J. Sun, C. Bian, J. Tong, and S. Xia, Micro Nano Lett. 7 (2012) 1197.
[17] G. Sharma, D. Kumar, A. Kumar, H. Ala'a, D. Pathania, M. Naushad, and G.T. Mola, Mater. Sci. and Eng. C. 71 (2017) 1216.
[18] A.A. Ahmed, T.S. Aldeen, S.A. Al-Aqil, Z.M. Alaizeri, and S. Megahed, ACS omega. 7 (2022) 37340.
[19] F.A. Zadeh, D. O. Bokov, O.D. Salahdin, W.K. Abdelbasset, M.A. Jawad, M.M. Kadhim, and M. Khatam, Rendiconti Lincei. Scienze Fisiche e Naturali 33 (2022) 441.
[20] A. Binod, S.V. Ganachari, J.S. Yaradoddi, R.P. Tapaskar, N.R. Banapurmath, and A.S. Shettar, IOP Publishing 376 (2018) 012054.
[21] M.B. Shivaswamy, P. Karthikdev, B.S. Madhukar, B.S. Hemanth, M.J. Deviprasad, R. Kavya, M.A. Sangamesha, A.P. Anand, H.P. Spoorthy, H.S. Nagendra Prasad, Chem. Inorg. Mater. 2 (2024) 100042.
[22] G.H. Hwang, W.K. Han, S.J. Kim, S.J. Hong, J.S. Park, H.J. Park, and S.G. Kang, JCPR 10 (2009) 190.
[23] R. Dobrucka, Int. J. Environ. Anal. Chem. 101 (2021) 2046.
[24] J. Miao, Z. Jia, H.B. Lu, D. Habibi, and L.C. Zhang, J. Taiwan Inst. Chem. Eng. 45 (2014) 1636.
[25] A.D. Faisa, A.A. Aljubouri, and W.K. Khalef, JASE 23 (2020) 461.
[26] M. Nyoka, Y.E. Choonara, P. Kuma, P.P. Kondiah, and V. Pillay, Nanomaterials 10 (2020) 242.
[27] Z. Vaseghi, O. Tavakoli, and A. Nematollahzadeh, J. Environ. Chem. Eng. 6 (2018) 1898.
[28] J. Ramyadev, K. Jeyasubramanian, A. Marikani, G. Rajakumar, A.A. Rahuman, T. Santhoshkumar, A.V. Kirthi, C. Jayaseelan, and S. Marimuthu, Parasitol. Res. 109 (2011) 1403.

[29] G. Jayakumar, A. Albert Irudayaraj, and A. Dhayal Raj, Opt. Quantum Electron. 51 (2019) 312.
[30] Z.M. Alaizer, H.A. Alhadlaq, S. Aldawood, M.J. Akhtar, and M. Ahamed, Environ Sci Pollut. Res. Int. 30 (2023) 6055.
[31] M.D. Nanjappa, and G.K. Jayaprakash, J. Electrochem. Sci. Eng. 13 (2023) 437.
[32] S. Adhav, S. Gaikwad, M. Nimse, and A. Rajbhoj, J. Clust. Sci. 22 (2011) 121.
[33] B.S. Hemanth, M.J. Deviprasad, M.B. Shivaswamy, H.S. Nagendra Prasad, S. Sumathi, R. Aswathy, M.A. Sangamesha, A.P. Ananda, H.S. Jayanth, and T.N. Lohith, J. Mol. Struct. 1310 (2024) 138240.
[34] S. Metwally, and U. Stachewicz, Mater. Sci. Eng. C 104 (2019) 109883.
[35] V. Sudha, G. Murugadoss, and R. Thangamuthu, Sci. Rep. 11 (2021) 3413.
[36] M.P. Ujwal, S.R. Yashas, H.P. Shivaraju, and N.K. Swamy, Surfaces and Interfaces 30 (2022) 101878.
[37] R.K.A. Amali, H.N. Lim, I. Ibrahim, N.M. Huang, Z. Zainal, and S.A.A. Ahmad, TrEAC 31 (2021) e00135.
[38] A. Adiraju, R. Munjal, Viehwege, A. Al-Hamry, A. Brahem, J. Hussain, and O. Kanoun, Sensors 23 (2023) 2961.
[39] Y. Suresh, S. Annapurna, G. Bhikshamaia, and A.K. Singh, IOP Publishing 149 (2016) 012187.
[40] M.F. Sanakousar, V.M. Jiménez-Pérez, B.K. Jayanna, A.H. Shridhar, and K. Prakash, J. Hazard. Mater. 2 (2021) 100004.
[41] A.M. Atta, Y.M. Moustafa, H.A. Lohedan, A.O. Ezzat, and A.I. Hashem, ACS Omega 5 (2020) 2829.
[42] R. Tomar, A.A. Abdala, R.G. Chaudhary, and N.B. Singh, Mater. Today 29 (2020) 967.
[43] H.S. Nagendra Prasad, A.P. Ananda, A. Mukarambi, N. Gaonkar, S. Sumathi, H. Spoorthy, and P. Mallu, Curr. Chem. Lett. 12 (2023) 65.
[44] V. Rajagopalan, Scientific Reports 6 (2016) 1.